IEEE Transactions on Robotics and Automation, Vol 12, No 5, October 1996.

Measurement and Correction of Systematic Odometry Errors in Mobile Robots

by
Johann Borenstein and Liqiang Feng
The University of Michigan
Advanced Technologies Lab, 1101 Beal Ave.
Ann Arbor, MI 48109-2110
Corresponding author: Johann Borenstein
Ph.: (313) 763-1560, Fax: (313) 944-1113, Email: johannb@umich.edu

ABSTRACT

Odometry is the most widely used method for determining the momentary position of a mobile robot. In most practical applications odometry provides easily accessible real-time positioning information in-between periodic absolute position measurements. The frequency at which the (usually costly and/or time-consuming) absolute measurements must be performed depends to a large degree on the accuracy of the odometry system.

This paper introduces practical methods for measuring and reducing odometry errors that are caused by the two dominant error sources in differential-drive mobile robots: (a) uncertainty about the effective wheelbase and (b) unequal wheel diameters. These errors stay almost constant over prolonged periods of time. Performing an occasional calibration as proposed here will increase the robot's odometric accuracy and reduce operation cost because an accurate mobile robot requires fewer absolute positioning updates. Many manufacturers or end-users calibrate their robots, usually in a time-consuming and non-systematic trial and error approach. By contrast, the method described in this paper is systematic, provides near-optimal results, and it can be performed easily and without complicated equipment.

Experimental results are presented that show a consistent improvement of at least one order of magnitude in odometric accuracy (with respect to systematic errors) for a mobile robot calibrated with our method.

Some parts of the material in this paper were presented at the 1995 International Conference on Intelligent Robots and Systems (IROS '95), Pittsburgh, Pennsylvania, August 5-9, 1995; some other parts were presented at the 1995 SPIE Conference on Mobile Robots, Philadelphia, October 22-26, 1995.

1. INTRODUCTION

In most mobile robot applications two basic position-estimation methods are employed together: absolute and relative positioning [Borenstein and Koren, 1987; Hollingum, 1991; Byrne et al., 1992; Chenavier and Crowley, 1992; Evans, 1994]. Relative positioning is usually based on odometry (i.e., monitoring the wheel revolutions to compute the offset from a known starting position). Odometry is simple, inexpensive, and easy to accomplish in real-time. The disadvantage of odometry is its unbounded accumulation of errors. A very comprehensive survey on mobile robot positioning methods is given in [Borenstein et al., 1996].

1.1 Absolute Positioning Methods

Absolute positioning methods usually rely on (a) navigation beacons, (b) active or passive landmarks, (c) map matching, or (d) satellite-based navigation signals. Each of these absolute positioning approaches can be implemented by a variety of methods and sensors. Yet, none of the currently existing systems is particularly elegant. Navigation beacons and landmarks usually require costly installations and maintenance, while map-matching methods are usually slower than odometry and the current techniques are not sufficiently robust yet to allow general commercial applications. With any one of these measurements it is necessary that the work environment either be prepared or be known and mapped with great precision. Satellite-based navigation (GPS) can be used only outdoors and has poor accuracy, on the order of 10-30 meters [Byrne, 1993]. Radio frequency-based systems are very expensive and are susceptible to reflections from metal objects [Byrne et al., 1992].

1.2 Inertial and Magnetic Positioning Methods

Another approach to the position determination of mobile robots is based on inertial navigation with gyros and/or accelerometers. Our own experimental results with this approach, as well as the results published by Barshan and Durrant-Whyte [1993, 1994], indicate that this approach is not advantageous. Accelerometer data must be integrated twice to yield position, thereby making these sensors exceedingly sensitive to drift. Another problem is that accelerations under typical operating conditions can be very small, on the order of 0.01 g. Yet, fluctuation of this magnitude already occur if the sensor tilts relative to a perfectly horizontal position by only 0.5^{o}, for example when the vehicle drives over uneven floors. Gyros can be more accurate (and costly) but they provide information only on the rate of rotation of a vehicle, so their data must be integrated once. This problem does not exist with electronic compasses that measure the orientation of the robot relative to the earth's magnetic field. However, electronic compasses are not recommended for indoor applications, because of the large distortions of the earth's magnetic field near power lines or steel structures [Byrne et al., 1992].

1.3 The Importance of Odometry

Improved odometry can dramatically reduce the cost for installations of mobile robot systems because it simplifies the fundamental problem of position determination. However, little research is directly aimed at improving the odometric accuracy of mobile robots. We attribute this observation to the fact that a large portion of research in mobile robotics is being done by the Artificial Intelligence (AI) community. AI researchers are traditionally concerned with the higher-level aspects of robotics. For this reason, AI researchers appear to focus on methods of feature extraction and map matching [Skewis et al., 1991; Kortenkamp et al. 1992; Rencken, 1994]. These research issues are of great importance for the future development of mobile robots, but at this time they are too slow to replace odometry altogether. Even Cox [1991], a proponent of map-matching, says about the virtues of odometric accuracy:

> "There also appears to be a self sustaining property to this configuration [map-matching combined with odometry]: Accurate knowledge of position allows for fast robust matching, which leads to accurate knowledge of position."

The well known disadvantage of odometry is that it is inaccurate with an unbounded accumulation of errors. Typical odometry errors will become so large that the robot's internal position estimate is totally wrong after as little as 10 m of travel [Gourley and Trivedi, 1994]. This paper helps reduce such problems as it introduces a systematic calibration method designed for the reduction of odometry errors.

2. Properties Of Odometry Errors

Figure 1 shows a typical differential drive mobile robot, the LabMate platform manufactured by [TRC]. In this design incremental encoders are mounted onto the two drive motors to count the wheel revolutions. Using simple geometric equations, it is straight-forward to compute the momentary position of the vehicle relative to a known starting position. This computation is called odometry. Odometry computes the robot's relative horizontal displacement and change in orientation as a function of the incremental horizontal displacement of the drive wheels. The latter is found from incremental wheel encoders as follows:

Suppose that at sampling interval I the left and right wheel encoders show a pulse increment of N_L and N_R, respectively. Suppose further that

$$c_m = \pi D_n / n C_e \qquad (2.1)$$

where

c_m - Conversion factor that translates encoder pulses into linear wheel displacement.

D_n - Nominal wheel diameter (in mm).

C_e - Encoder resolution (in pulses per revolution).

n - Gear ratio of the reduction gear between the motor (where the encoder is attached) and the drive wheel.

One can then compute the incremental travel distance for the left and right wheel, $\Delta U_{L,i}$ and $\Delta U_{R,i}$ according to

$$\Delta U_{L/R,\,i} = c_m N_{L/R,\,i} \qquad (2.2)$$

We omit here the detailed development of the well known odometry equations for differential drive vehicles. These equations can be found in [Borenstein et al., 1996] or [Crowley and Reignier 1992].

Odometry is based on simple equations that are easily implemented and that utilize data from inexpensive incremental wheel encoders. However, odometry is based on the assumption that wheel revolutions can be translated into linear displacement relative to the floor. This assumption is only of limited validity. One extreme example is wheel slippage: If one wheel was to slip on, say, an oil spill, then the associated encoder would register wheel revolutions even though these revolutions would not correspond to a linear displacement of the wheel.

Besides this extreme case of total slippage, there are several other, more subtle reasons for inaccuracies in the translation of wheel encoder readings into linear motion. All of these error sources fit into one of two categories: (1) systematic errors and (2) non-systematic errors.

1. Systematic errors

a. Unequal wheel diameters
b. Average of both wheel diameters differs from nominal diameter
c. Misalignment of wheels
d. Uncertainty about the effective wheelbase (due to non-point wheel contact with the floor)
e. Limited encoder resolution
f. Limited encoder sampling rate

2. Non-systematic errors

a. Travel over uneven floors
b. Travel over unexpected objects on the floor
c. Wheel-slippage due to:

- slippery floors
- over-acceleration
- fast turning (skidding)
- external forces (interaction with external bodies)

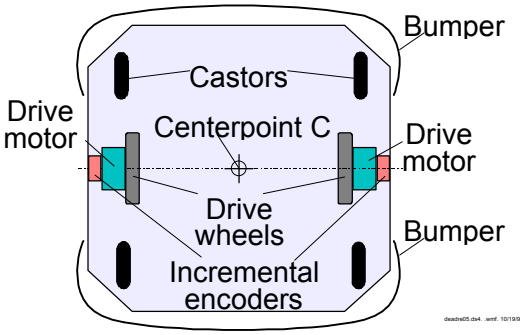

Figure 1: A typical differential-drive mobile robot (bottom view).

- internal forces (e.g., castor wheels)
- non-point wheel contact with the floor

Systematic errors are particularly grave, because they accumulate constantly. On most smooth indoor surfaces systematic errors contribute much more to odometry errors than non-systematic errors. However, on rough surfaces with significant irregularities, non-systematic errors may be dominant.

Additional odometry errors can be introduced through the odometry equations themselves, since they approximate arbitrary motion as a series of short straight line segments. The precision of this approximation depends on the sampling frequency with respect to the speed of the robot. In our practical experience, however, this error is negligible when working with typical sampling times of $T_s < 10$ ms and typical speeds of $V < 1$ m/s.

Finally, we note that in order to reduce overall odometry errors, orientation errors are the main source of concern because once they are incurred they grow without bound into lateral position errors [Crowley, 1989; Feng et al., 1993].

2.1 Non-Systematic Odometry Errors

Non systematic odometry errors are those errors that are caused by interaction of the robot with unpredictable features of the environment. For example, irregularities of the floor surface, such as bumps, cracks, or debris, will cause a wheel to rotate more than predicted by Eq. (2.2), because the affected wheel travels up or down the irregularity, in addition to the — expected — horizontal amount of travel. Non-systematic errors are a great problem for actual applications, because it is impossible to predict an upper bound for the odometry error. Recent work at the University of Michigan [Borenstein, 1994; 1995a; 1995b] showed that by using redundant encoder data, non-systematic errors can be reduced by orders of magnitude. However, in the present paper we will concentrate on the treatment of systematic errors.

2.2 Systematic Odometry Errors

Systematic errors are vehicle-specific and don't usually change during a run (although different load distributions can change some systematic errors quantitatively). Thus, odometry can be improved generally (and in our experience, significantly) by measuring the individual contribution of the most dominant errors sources, and then counter-acting their effect in software.

Systematic errors are usually caused by imperfections in the design and mechanical implementation of a mobile robot. In the course of over 12 years of experimental work with differential-drive mobile robots we observed that the two most notorious systematic error sources are unequal wheel diameters and the uncertainty about the effective wheelbase. This opinion is reflected in the literature, where these two error sources are named most often [Borenstein and Koren,

1985; 1987; Crowley, 1989; Komoriya and Oyama, 1994; Everett, 1995].

a) Unequal wheel diameters. Most mobile robots use rubber tires to improve traction. These tires are difficult to manufacture to exactly the same diameter. Furthermore, rubber tires compress differently under asymmetric load distribution. Either one of these effects can cause substantial odometry errors. We will denote this error as E_d and we define it as

$$E_d = D_R/D_L \tag{2.3}$$

where D_R and D_L are the actual wheel diameters. The nominal ratio between the wheel diameters is of course 1.00.

b) Uncertainty about the wheelbase. The wheelbase is defined as the distance between the contact points of the two drive wheels of a differential-drive robot and the floor. The wheelbase must be known in order to compute the number of differential encoder pulses that correspond to a certain amount of rotation of the vehicle. Uncertainty in the effective wheelbase is caused by the fact that rubber tires contact the floor not in one point, but rather in a contact area. The resulting uncertainty about the effective wheelbase can be on the order of 1% in some commercially available robots. We will denote this error as E_b and we define it as

$$E_b = b_{actual}/b_{nominal} \tag{2.4}$$

where b is the wheelbase of the vehicle.

It is important to note that E_b has an effect only when turning, while E_d affects only straight line motion. E_d and E_b are dimensionless values, expressed as fractions of the nominal value.

At this time we have defined only the wheelbase error, E_b, and the ratio between actual wheel diameters, E_d, as relevant factors. However, if the average of the two actual wheel diameters, denoted D_a, differs from the nominal wheel diameter, denoted D_n, then the vehicle will experience an additional odometry error, which we call the scaling error E_s. E_s affects straight-line motion and, as we will show in Section 2.3, pure turning motion. However, even though E_s can be a significant error, E_s is exceedingly easy to measure with just an ordinary tape measure. For this reason we will assume that E_s has been measured and corrected in software before any of the procedures described in this paper is performed.

2.3 The Effect of Unequal Wheel-diameters During Turning

In this Section we investigate how unequal wheel diameters affect on-the-spot turning of a differential-drive mobile robot. The results of this section are of fundamental importance for the odometry error measuring and correction methods discussed later.

Figure 2 shows the two drive wheels of the robot before and after a nominal turn τ_n. Since on-the-spot-turning requires that both wheels rotate at the same speed, we can assume that the angular velocity of both wheels is equal. However, due to the unequal wheel diameters the actual linear velocities of the wheels are proportional to the actual wheel diameters D_R and D_L. Thus, the

instantaneous center of rotation (ICR) 'O' can be found easily as shown in Fig. 2. Note that 'O' does not coincide with the vehicle centerpoint C. At the completion of this turn point C will have moved to C'. The "on-the-spot" turn is therefore accompanied by a lateral displacement. However, in the square path experiment with four "on-the-spot" turns the four resulting lateral displacements balance and can be ignored.

We now wish to derive a relation between the actual wheel diameters D_L and D_R, and the actual angle of rotation τ. From Fig. 2 we obtain

$$\frac{r_R}{r_L} = \frac{D_R}{D_L} \tag{2.5}$$

where $r_{R/L}$ is the distance from the ICR 'O' to the right or left wheel.

Next, rewriting Eq. (2.5) yields

$$r_R = (D_R/D_L)\, r_L \tag{2.6}$$

Under normal driving conditions the ICR is always on the drive axis (or along its imaginary extension beyond the wheels), so that

$$r_R + r_L = b \tag{2.7}$$

Substituting Eq. (2.6) into Eq. (2.7) and solving for r_L yields

$$r_L = \frac{D_L}{D_R + D_L} b \tag{2.8}$$

Let us denote the nominal curvelinear displacement of the left wheel as $U_{L,n}$. Let us further denote the nominal diameter of the left wheel as $D_{L,n}$ and the number of rotations of the left wheel as N_L.

Then

$$U_{L,n} = \pi\, D_{L,n}\, N_L \tag{2.9}$$

Under nominal conditions, the left wheel would be turning around C with an angle τ_n

$$t = \frac{U_{L,n}}{b/2} = \frac{2pN_L D_{L,n}}{b}$$

Now let us suppose that the right wheel was smaller than the left one. The rotation is now about point C' in Fig. 2 and the angle corre-

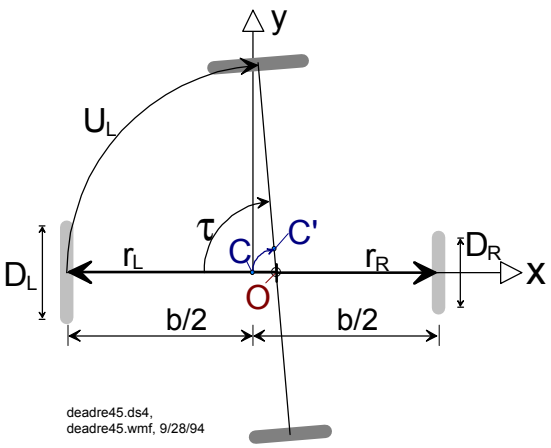

Figure 2: When turning through a nominal angle n, it is not the "unequal wheel diameter" error, but rather the "average actual wheel diameter" error, that affects the amount of turning.

sponding to its curvelinear displacement is:

$$t = \frac{U_L}{r_L} = \frac{pN_L D_L}{r_L} \tag{2.11}$$

Solving Eq. (2.10) for N_L and substituting in Eq. (2.11) yields

$$t = \frac{t_n b D_L}{2 r_L D_{L,n}} \tag{2.12}$$

Substituting Eq. (2.8) in Eq. (2.12) yields:

$$t = t_n \frac{D_R + D_L}{2 D_{L,n}} \tag{2.13}$$

To interpret this result more easily, we define the average actual wheel diameter

$$D_{avrg} = \frac{D_R + D_L}{2} \tag{2.14}$$

and we rewrite Eq. (2.14) as

$$\frac{D_{avrg}}{t} = \frac{D_{L,n}}{t_n} \tag{2.15}$$

Equation (2.15) can be expressed in words as "The average actual wheel diameter relates to the actual angle of turning as the nominal wheel diameter relates to the nominal angle of turning."

Three important conclusions can be drawn from Eq. (2.15):

1. Unequal wheel diameters do not cause an orientation error during turning.
2. Whatever E_d is, $\tau = \tau_n$ if $(D_R + D_L)/2 = D_n$. In other words, the orientation error depends on the average actual wheel diameter $D_{avrg} = (D_L+D_R)/2$. If $D_{avrg} > D_n$, then the vehicle will turn more than the nominal amount. If $D_{avrg} < D_n$, then the vehicle will turn less.
3. E_d has a minor effect on the x and y position of centerpoint C, because the actual center of rotation, C', does not coincide with C, as shown in Fig. 2.

3. MEASUREMENT OF SYSTEMATIC ODOMETRY ERRORS

In this section we introduce methods for isolating and measuring systematic odometry errors. We discuss two test sequences (benchmark tests), which allow the experimenter to draw conclusions about the overall odometric accuracy of the robot, and to compare the performance of different mobile robots from different manufacturers.

The first benchmark test is called the "uni-directional square path" test. This test, or some variations of this test, have been mentioned in the literature [Cybermotion, 1988; Komoriya and

Oyama, 1994], but we will show that this test is unsuitable for differential drive vehicles. To overcome the shortcomings of the uni-directional square path test, we will later introduce in Section 3.2 a benchmark test called the "bi-directional square path test."

3.1 The uni-directional square path as a benchmark test

Figure 3a shows a 4×4 m uni-directional square path. The robot starts out at a position x_0, y_0, θ_0, which is labeled START. The starting area should be located near the corner of two perpendicular walls. The walls serve as a fixed reference before and after the run: measuring the distance between three specific points on the robot and the walls allows accurate determination of the robot's absolute position and orientation.

The robot is programmed to traverse the four legs of the square path. The path will return the vehicle to the starting area, but, because of odometry and controller errors, not precisely to the starting position. Since this test aims at determining odometry errors and not controller errors, the vehicle does not need to be programmed to return to its starting position precisely — returning approximately to the starting area is sufficient. Upon completion of the square path, the experimenter again measures the absolute position of the vehicle, using the fixed walls as a reference. These absolute measurements are then compared to the position and orientation of the vehicle as computed from odometry data. The result is a set of return position errors caused by odometry and denoted ϵx, ϵy, and $\epsilon\theta$.

$$\begin{aligned} \epsilon x &= x_{abs} - x_{calc} \\ \epsilon y &= y_{abs} - y_{calc} \\ \epsilon\theta &= \theta_{abs} - \theta_{calc} \end{aligned} \tag{3.1}$$

where

ϵx, ϵy, $\epsilon\theta$ — Position and orientation errors due to odometry.
x_{abs}, y_{abs}, θ_{abs} — Absolute position and orientation of the robot.
x_{calc}, y_{calc}, θ_{calc} — Position and orientation of the robot as computed from odometry.

The path shown in Fig. 3a comprises of four straight line segments and four pure rotations about the robot's centerpoint, at the corners of the square. The robot's end position shown in Fig. 3a visualizes the dead-reckoning error.

While analyzing the results of this experiment, the experimenter may draw two different conclusions: (1) The odometry error is the result of unequal wheel diameters, E_d, as shown by the slightly curved trajectory in Fig. 3b (dotted line); or, (2) the odometry error is the result of uncertainty about the wheelbase, E_b. In the example of Fig. 3b, E_b caused the robot to turn 87° instead of the desired 90° (dashed trajectory in Fig. 3b).

As one can see in Fig. 3b, either one of these two cases could have yielded approximately the same position error. The fact that two different error-mechanisms can result in the same overall error may lead an experimenter toward a serious mistake: correcting only one of the two error sources in software. This mistake is so serious because it will yield apparently "excellent" results, as shown in the example in Fig. 4. In this example, we assume that the experimenter began "improving" performance by adjusting the wheelbase b in the control software. The experimenter needs only to increase the value of b to make the robot turn more in each nominal 90° turn. In doing so, the experimenter will soon have adjusted b to what appears to be the "ideal" value, namely, the one that will cause the robot to turn 93°, thereby effectively compensating for the 3° orientation error introduced by each slightly curved (but nominally straight) leg of the square path. Obviously, the thus "calibrated" robot would incur huge odometry errors, even though the uni-directional calibration procedure showed that the robot was calibrated well.

We should note that another popular test path, the "figure-8" path [Tsumura et al., 1981; Borenstein and Koren, 1985, Cox 1991] can be shown to have the same shortcomings as the uni-directional square path.

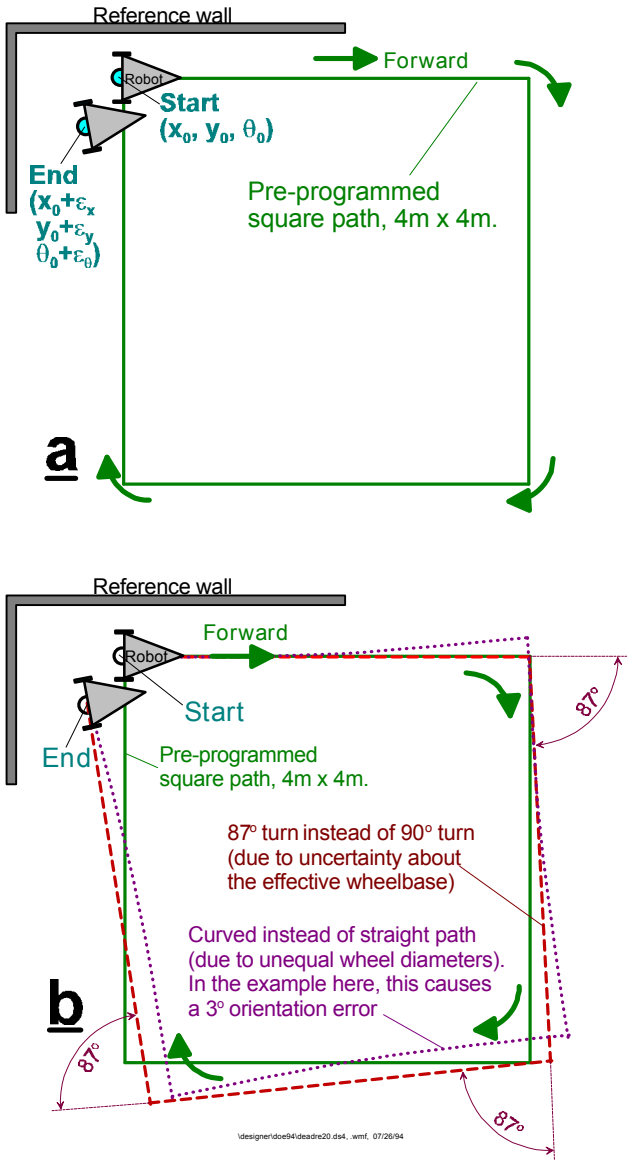

Figure 3: The unidirectional square path experiment.
a. The nominal path.
b. Either one of the two significant errors E_b or E_d can cause the same final position error.

3.2 The bi-directional square path experiment: "UMBmark"

The detailed example of the preceding section illustrates that the uni-directional square path experiment is unsuitable for testing odometry performance, because it can easily conceal two mutually compensating odometry errors. To overcome this problem, we introduce the Bi-

directional Square Path experiment, called University of Michigan Benchmark (UMBmark). UMBmark requires that the square path experiment be performed in both clockwise and counter-clockwise direction. Figure 5 shows that the concealed dual-error from the example in Fig. 4 becomes clearly visible when the square path is performed in the opposite direction. This is so because the two dominant systematic errors, which may compensate for each other when run in only one direction, add up to each other and increase the overall error when run in the opposite direction.

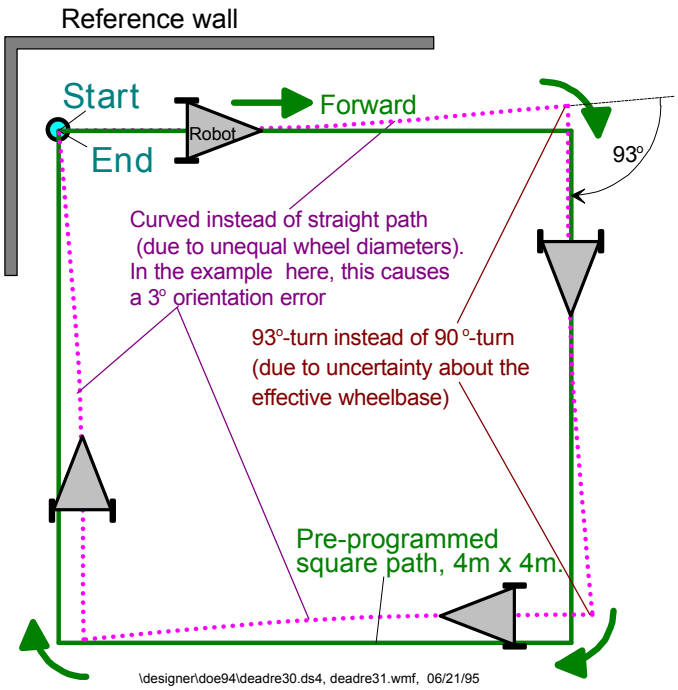

Figure 4: The effect of the two dominant systematic odometry errors E_b and E_d. Note how both errors may cancel each other out when the test is performed in only one direction.

The result of the Bi-directional Square Path experiment might look similar to the one shown in Fig. 6, which shows actual results with an off-the-shelf LabMate robot carrying an evenly distributed load. In this experiment the robot was programmed to follow a 4×4 m square path, starting at (0,0). The stopping positions for five runs each in clockwise (cw) and counter-clockwise (ccw) directions are shown in Fig. 6. Note that Fig. 6 is an enlarged view of the target area. The results of Fig. 6 can be interpreted as follows:

a. The stopping positions after cw and ccw runs are clustered in two distinct areas.

b. The distribution within the cw and ccw clusters are the result of non-systematic errors, as mentioned in Section 2.1. However, Fig. 6 shows that in an uncalibrated vehicle traveling over a reasonably smooth concrete floor, the contribution of systematic errors to the total odometry error is notably larger[1] than the contribution of non-systematic errors.

After conducting the UMBmark experiment, one may wish to derive a single numeric value that expresses the odometric accuracy (with respect to systematic errors) of the tested vehicle. In order to minimize the effect of non-systematic errors, we suggest to consider the center of gravity of each cluster as representative for the odometry errors in cw and ccw directions. The coordinates of the two centers of gravity are computed from the results of Eq. (3.1) as

[1]In informal tests with two other LabMate robots at our lab we have observed (but not methodically noted) even greater systematic odometry errors than those in Fig. 6. These may be due to less balanced load-distributions in those earlier tests.

$$x_{c.g.,cw/ccw} = \frac{1}{n}\sum_{i=1}^{n} e\, x_{i,cw/ccw} \qquad (3.2)$$

$$y_{c.g.,cw/ccw} = \frac{1}{n}\sum_{i=1}^{n} e\, y_{i,cw/ccw}$$

where n = 5 is the number of runs in each

The absolute offsets of the two centers o
$_{ccw}$ (see Fig. 6) and are given by

$$r_{c.g.,cw} = \sqrt{(x_{c.g.,cw})^2 + (y_{c.g.,cw})^2}$$

and (3.3)

$$r_{c.g.,ccw} = \sqrt{(x_{c.g.,ccw})^2 + (y_{c.g.,ccw})^2}$$

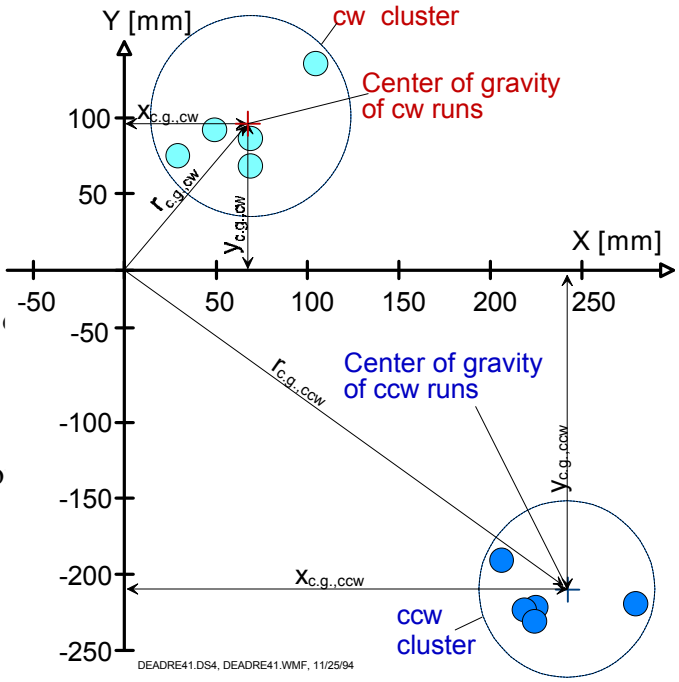

Figure 5: Typical results from running UMBmark (a square path run in both cw and ccw directions) with an uncalibrated vehicle.

Finally, we define the larger value among $r_{c.g.,\,cw}$ and $r_{c.g.,\,ccw}$ as the measure of odometric accuracy for systematic errors

$$E_{max,syst} = \max(r_{c.g.,cw}\ ;\ r_{c.g.,ccw}) \qquad (3.4)$$

The reason for not using the average of the two centers of gravity $r_{c.g.,cw}$ and $r_{c.g.,ccw}$ is that for practical applications, one needs to worry about the largest possible odometry error. Note that the final orientation error $\epsilon\theta$ is not considered explicitly in the expression for $E_{max,syst}$. This is so because all systematic orientation errors are implied by the final position errors. In other words, since the square path has fixed-length sides, systematic orientation errors translate directly into position errors (as will be shown by Eq. (4.8) and (4.16) in Section 4).

3.3 Summary of the UMBmark Procedure

In summary, the UMBmark is defined as the following procedure:

1. At the beginning of the run, measure the absolute position (and, optionally, orientation) of the vehicle and initialize the onboard odometric starting position to that position.

2. Run the vehicle through a 4×4 m square path in cw direction, making sure to

   - stop after each 4 m straight leg;
   - make a total of four 90°-turns on the spot;
   - run the vehicle slowly to avoid slippage.

3. Upon return to the starting area, measure the absolute position (and, optionally, orientation) of the vehicle.

4. Compare the absolute position to the robot's calculated position, based on odometry and using Eqs. (3.1).

5. Repeat steps 1-4 for four more times (i.e., a total of five runs).

6. Repeat steps 1-5 in ccw direction.

7. Use Eqs. (3.2) and (3.3) to express the experimental results quantitatively as the measure of odometric accuracy for systematic errors, $E_{max,syst}$.

8. Optionally, use a plot similar to Fig. 6 to represent ϵx_i and ϵy_i graphically.

4. CORRECTION OF SYSTEMATIC ODOMETRY ERRORS

One interesting aspect of the error distribution pattern in the UMBmark experiment (see Fig. 6, above) is the fact that one can analytically derive correction factors from the experimental results. Before we do so, let us first define two new error characteristics that are meaningful only in the context of the Bi-directional Square Path experiment. These characteristics, called Type A and Type B, represent odometry errors in orientation. Type A is defined as an orientation error that reduces (or increases) the total amount of rotation of the robot during the square path experiment in both cw and ccw direction. By contrast, Type B is defined as an orientation error that reduces (or increases) the total amount of rotation of the robot during the square path experiment in one direction, but increases (or reduces) the amount of rotation when going in the other direction. As examples consider Figures 7 and 8, below.

Figure 7 shows a case where the robot turns four times for a nominal amount of 90° per turn. However, because the actual wheelbase of the vehicle was larger than the nominal value, the vehicle actually turned only 85° in each corner of the square path. In the example of Fig. 7 the robot will actually turn only $\theta_{total} = 4 \times 85^o = 340^o$, instead of the desired $\theta_{nominal} = 360^o$. We observe that in both the cw and the ccw experiment the robot ends up turning less than the desired amount , i.e., $|\theta_{total,cw}| < |\theta_{nominal}|$ and $|\theta_{total,\ ccw}| < |\theta_{nominal}|$. Thus, the orientation error is of Type A.

In Fig. 8 the trajectory of a robot with unequal wheel diameters is shown. This error expresses

itself in a curved path that adds to the overall orientation at the end of the run in ccw direction, but it reduces the overall rotation in the ccw direction, i.e., $|\theta_{total,\ ccw}| > |\theta_{nominal}|$ but $|\theta_{total,\ cw}| < |\theta_{nominal}|$. Thus, the orientation error in Fig. 8 is of Type B.

In an actual run Type A and Type B errors will of course occur together. The problem is therefore how to distinguish and compute Type A and Type B errors from the measured final position errors of the robot in the Bi-directional Square Path experiment. We approach this problem by defining the following simplified model for systematic odometry errors:

Assumptions:

1. E_d and E_b are the dominant sources of systematic odometry errors.
2. An incorrect wheelbase (E_b) causes errors only during turning but not during straight line motion.
3. Unequal wheel diameters (E_d) cause errors only during straight line motion but not during turning.
4. E_b causes only Type A errors but not Type B errors.
5. E_d causes only Type B errors but not Type A errors.

Consequences:

1. Because of assumption #1, eliminating E_b eliminates the system's Type A error almost completely.
2. Because of assumption #1, eliminating E_d eliminates the system's Type B error almost completely.

Because of the close association between E_b and Type A errors and between E_d and Type B errors (according to assumptions #6 and #7) we will use the terms E_b and Type A, as well as the terms E_d and Type B, interchangeably.

4.1 Analysis of Type A and Type B Errors

Having defined a model, we will now analyze the characteristics of the UMBmark procedure with regard to that model. To simplify the mathematical treatment, we will make extensive use of approximations for small angles: $L\sin\gamma \approx L\gamma$ and $L\cos\gamma \approx L$. For simplicity, we assume that the starting position (x_0, y_0) of the robot is at (0,0). At first we will analyze and examine the contribution of Type A and Type B errors separately. Then, we will superimpose both errors to represent the actual conditions.

Figure 7 shows the contribution of Type A errors. We recall that according to assumptions #1 and #4 Type A errors are caused mostly by E_b. We also recall that Type A errors cause too much

or too little turning at the corners of the square path. The (unknown) amount of erroneous rotation in each nominal 90° turn is denoted as α. Due to the above approximations, α is measured in [rad].

a. For Type A errors in ccw direction:

$x_1 = x_0 + L$ (4.1a)

$y_1 = y_0$ (4.1b)

$x_2 = x_1 + L\sin\alpha \approx L + L\alpha$ (4.2a)

$y_2 = y_1 + L\cos\alpha \approx L$ (4.2b)

$x_3 = x_2 - L\cos 2\alpha \approx L\alpha$ (4.3a)

$y_3 = y_2 + L\sin 2\alpha \approx L + 2L\alpha$ (4.3b)

$x_4 = x_3 - L\sin 3\alpha \approx -2L\alpha$ (4.4a)

$y_4 = y_3 - L\cos 3\alpha \approx 2L\alpha$ (4.4b)

b. For Type A errors in cw direction:

$x_1 = x_0 + L$ (4.5a)

$y_1 = y_0$ (4.5b)

$x_2 = x_1 + L\sin\alpha \approx L + L\alpha$ (4.6a)

$y_2 = y_1 - L\cos\alpha \approx -L$ (4.6b)

$x_3 = x_2 - L\cos 2\alpha \approx L\alpha$ (4.7a)

$y_3 = y_2 - L\sin 2\alpha \approx -L - 2L\alpha$ (4.7b)

$x_4 = x_3 - L\sin 3\alpha \approx -2L\alpha$ (4.8a)

$y_4 = y_3 + L\cos 3\alpha \approx -2L\alpha$ (4.8b)

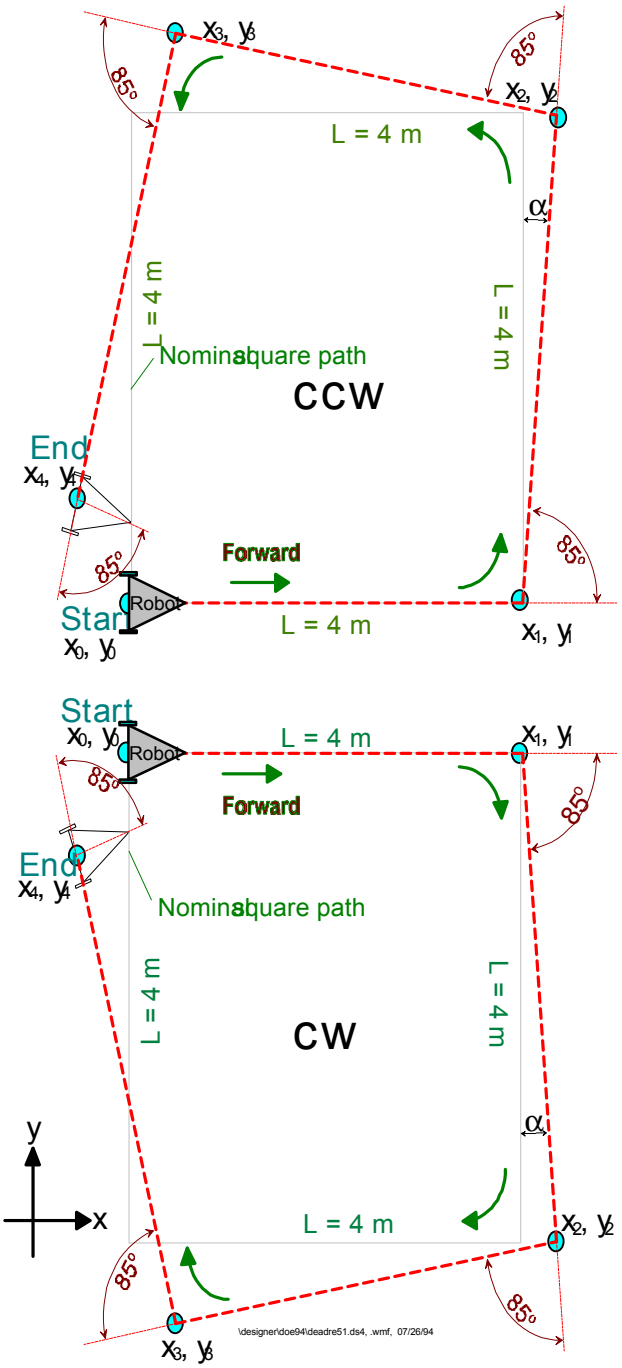

Figure 7: Type A errors in ccw and cw direction. Type A errors are caused only by the wheelbase error E_b.

Figure 8 shows the contribution of Type B errors. We recall that according to our assumptions #1 and #5 Type B errors are caused mostly by the ratio between wheel diameters, E_d. We also recall that Type B errors cause a slightly curved path instead of a straight one during the four straight legs of the square path. Because of the curved motion, the robot will have gained an incremental orientation error, denoted β,

at the end of each straight leg. Note that the auxiliary line c'_1, which connects the corner points of the actual path, has a slope of $\beta/2$ because it is parallel to the tangent to the midpoint of arc c_1. With respect to the unknown parameter β (in [rad]), we obtain:

a. For Type B errors in ccw direction:

$$x_1 = x_0 + L\cos(\beta/2) \approx L \quad (4.9a)$$

$$y_1 = y_0 + L\sin(\beta/2) \approx L\beta/2 \quad (4.9b)$$

$$x_2 = x_1 - L\sin(3\beta/2) \approx L - L\beta/2 \quad (4.10a)$$

$$y_2 = y_1 + L\cos(3\beta/2) \approx L\beta/2 + L \quad (4.10b)$$

$$x_3 = x_2 - L\cos(5\beta/2) \approx -3L\beta/2 \quad (4.11a)$$

$$y_3 = y_2 - L\sin(5\beta/2) \approx -2L\beta + L \quad (4.11b)$$

$$x_4 = x_3 + L\sin(7\beta/2) \approx 2L\beta \quad (4.12a)$$

$$y_4 = y_3 - L\cos(7\beta/2) \approx -2L\beta \quad (4.12b)$$

b. For Type B errors in cw direction:

$$x_1 = x_0 + L\cos(\beta/2) \approx L \quad (4.13a)$$

$$y_1 = y_0 + L\sin(\beta/2) \approx L\beta/2 \quad (4.13b)$$

$$x_2 = x_1 + L\sin(3\beta/2) \approx L + 3L\beta/2 \quad (4.14a)$$

$$y_2 = y_1 - L\cos(3\beta/2) \approx L\beta/2 - L \quad (4.14b)$$

$$x_3 = x_2 - L\cos(5\beta/2) \approx 3L\beta/2 \quad (4.15a)$$

$$y_3 = y_2 - L\sin(5\beta/2) \approx -L(2\beta + 1) \quad (4.15b)$$

$$x_4 = x_3 - L\sin(7\beta/2) \approx -2L\beta \quad (4.16a)$$

$$y_4 = y_3 + L\cos(7\beta/2) \approx -2L\beta \quad (4.16b)$$

Superimposing Type A and Type B errors for the cw experiment in x-direction yields x_{cw}:

$$-2L\alpha - 2L\beta = -2L(\alpha + \beta) = x_{c.g.,cw} \quad (4.17)$$

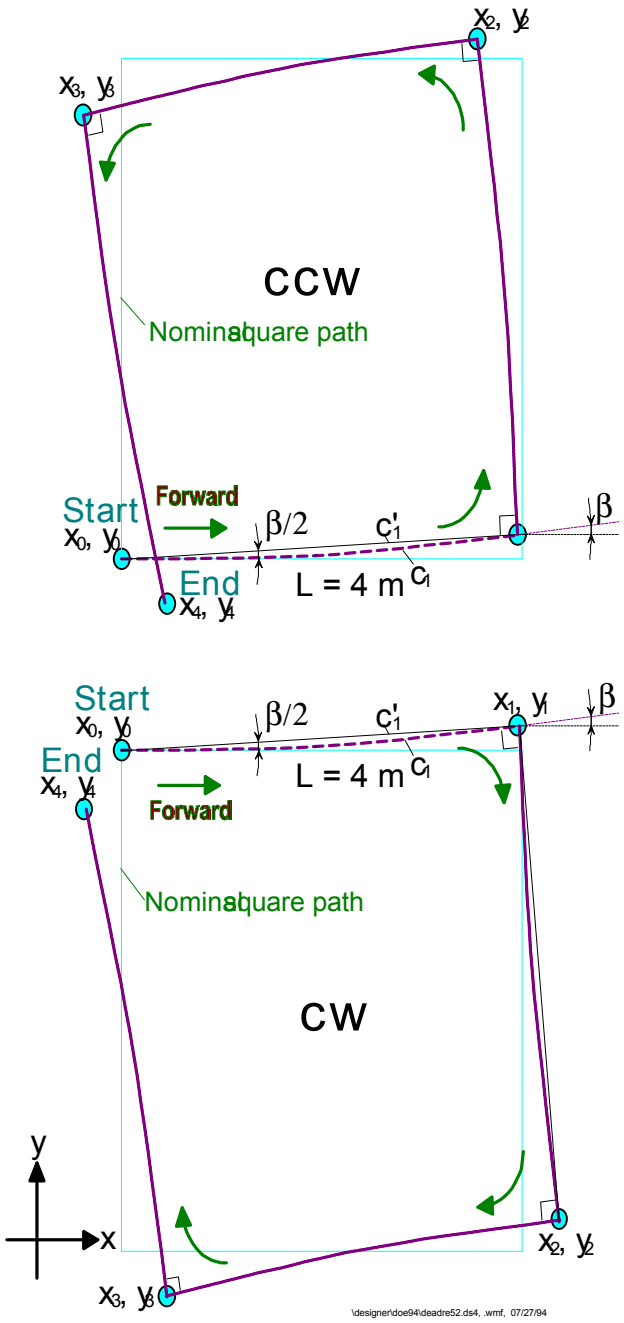

Figure 8: Type B errors in ccw and cw direction. Type B errors are caused only unequal wheel diameters E_d.

x_{ccw}:

$$-2L\alpha + 2L\beta = -2L(\alpha - \beta) = x_{c.g.,ccw} \qquad (4.18)$$

Subtracting (4.18) from (4.17) yields

$$-4L\beta = x_{c.g.,cw} - x_{c.g.,ccw}$$

or

$$b = \frac{(x_{c.g.,cw} - x_{c.g.,ccw})}{-4L}\frac{180^o}{p} \qquad (4.20a)$$

for β in degrees.

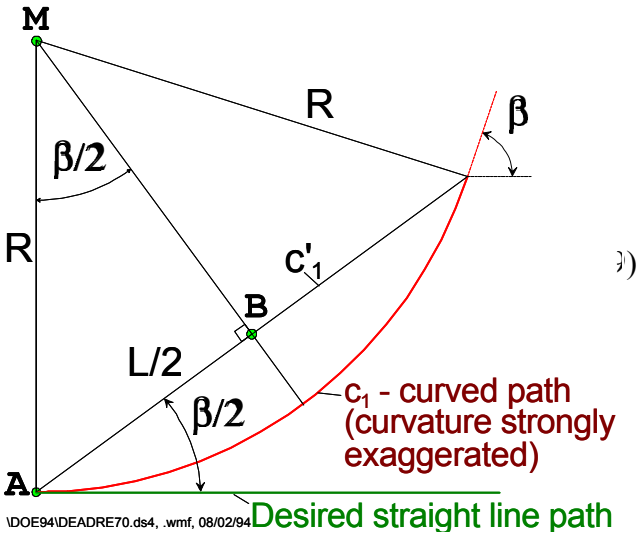

Figure 9: Geometric relations for finding the radius of curvature.

Comparing terms in y-direction yields a similar result

$$b = \frac{(y_{c.g.,cw} + y_{c.g.,ccw})}{-4L}\frac{180^o}{p} \qquad (4.20b)$$

Using simple geometric relations, the radius of curvature R of the curved path of Fig. 8 can be found from triangle ABM in Fig. 9.

$$R = \frac{L/2}{\sin(b/2)} \qquad (4.21)$$

Once radius R is computed, it is easy to determine the ratio between the two wheel diameters that caused the robot to travel on a curved, instead of a straight path (see Fig. 10):

$$E_d = \frac{D_R}{D_L}\frac{R + b/2}{R - b/2} \tag{4.22}$$

The ratio of Eq. (4.22) can be used to correct Type B errors as will be explained in Section 4.2.

Similarly, α can be found by adding Eq. (4.17) and Eq. (4.18)

$$-4L\alpha = x_{c.g.,cw} + x_{c.g.,ccw} \tag{4.23}$$

or

$$a = \frac{(x_{c.g.,cw} + x_{c.g.,ccw})}{-4L}\frac{180^o}{p} \tag{4.24a}$$

solves for α in [degrees].

Again, comparing terms in y-direction yields a similar result for α

$$a = \frac{(y_{c.g.,cw} - y_{c.g.,ccw})}{-4L}\frac{180^o}{p} \tag{4.24b}$$

We can now compute the wheelbase error E_b. Since the wheelbase b is inversely proportional to the actual amount of rotation (as shown by the well known odometry equations [Borenstein et al., 1996]), we can use the proportion:

$$\frac{b_{actual}}{90^o} = \frac{b_{nominal}}{90^o - a} \tag{4.25}$$

so that

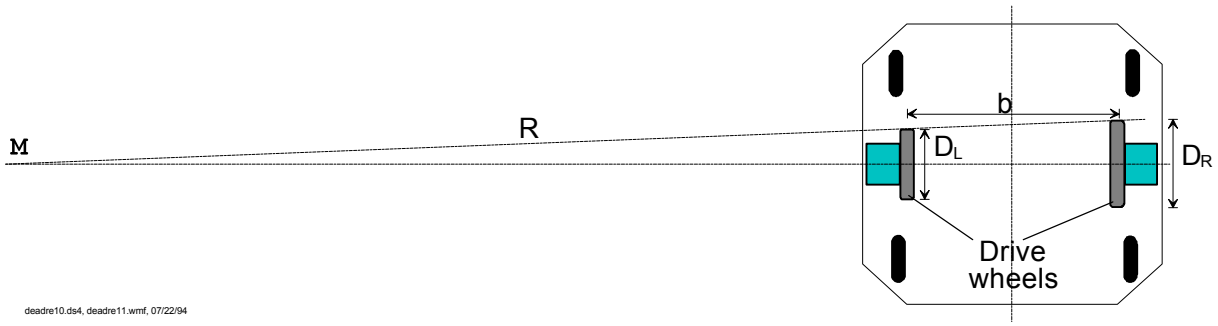

Figure 10: Unequal wheel diameters cause the robot to travel on a curved path of radius R (curvature is exaggerated for better illustration).

$$b_{actual} = \frac{90^o}{90^o - a} b_{nominal} \tag{4.26}$$

where, per odometry equations given in [Borenstein et al., 1996]

$$E_b = \frac{90^o}{90^o - a} \tag{4.27}$$

4.2 Compensation for systematic odometry errors

Once we know the quantitative values of E_d and E_b, it is easy to compensate for these errors in software. The correction for the wheelbase error E_b is trivial: the wheelbase b is redefined in software according to Eq. (4.26). The correction for the unequal wheel diameters, E_d, is slightly more complex: After performing the UMBmark procedure, we know the actual wheel diameter ratio $E_d = D_R/D_L$ from Eq. (4.22). However, when applying a compensation factor, we must make sure not to change the average wheel diameter D_a, since one would then have to recalibrate that parameter. D_a will remain unchanged if we consider it as a constraint

$$D_a = (D_R + D_L)/2 \tag{4.28}$$

Solving Eqs. (4.22) and (4.28) as a set of two linear equations with two unknowns, D_R and D_L, yields

$$D_L = \frac{2}{E_d + 1} D_a \tag{4.29}$$

and

$$D_R = \frac{2}{(1 / E_d) + 1} D_a \tag{4.30}$$

We can now define the two correction factors

$$c_L = \frac{2}{E_d + 1} \tag{4.31}$$

and

$$c_R = \frac{2}{(1 / E_d) + 1} \tag{4.32}$$

which can be implemented in the odometry algorithm by rewriting Eq. (2.2) as

$$\Delta U_{L/R,\,i} = c_{L/R}\, c_m\, N_{L/R,\,i} \qquad (4.33)$$

We have thus corrected both dominant systematic errors.

5. EXPERIMENTAL RESULTS

In this section we describe experiments that validate the above described method for correcting Type A and Type B errors by changing the effective wheelbase b and the effective wheel-diameter ratio D_R/D_L. The experiments were performed with a LabMate robot equipped with an onboard AMPRO 486/50 MHz PC compatible single-board computer.

The robot was programmed for both a cw and a ccw 4×4 m square path. To avoid slippage, the robot was traveling slowly, at a speed of 0.2 m/s during the straight legs of the square path. At the end of each leg the robot came to a complete stop and rotated on-the-spot through 90^o. This means that the robot made a fourth 90^o turn after returning to its starting area. The linear speed of the two drive wheels during turning was approximately 0.2 m/s and -0.2 m/s. The robot started and stopped near an L-shaped corner and used a so-called "sonar calibrator" [Borenstein 1993] to determine its position and orientation relative to the L-shaped corner. We will refer to this as the absolute position. The sonar calibrator comprises three standard POLAROID ultrasonic sensors. Two sensors were facing the long side of the L-shaped corner, the third sensor faced the short side. The ultrasonic sensor system allowed measurement of the absolute position of the vehicle to within ±2 millimeters in the x and y directions, and to about $\pm 0.4^o$ in orientation.

At the beginning of each run a sonar measurement was taken to determine the starting position of the vehicle. The robot then traveled through the programmed path and returned to the L-shaped corner, where the perceived position (i.e., the position the vehicle "thought" it had, based on odometry) was recorded. Then, a second sonar measurement was taken to determine the absolute position. The difference between the absolute position and the perceived position is the return position error ϵ, as defined by Eqs. (3.1), above.

The uncalibrated robot (i.e., $D_R/D_L = 1.0000$ and $b = b_{nominal} = 340.00$ mm) made five cw trips and five ccw trips. As expected, the return position errors were clearly grouped in a cw cluster and a ccw cluster, as was shown in Fig. 6. For each of the two clusters the x and y components of the respective centers of gravity were computed according to Eq. (3.2). The resulting $x_{c.g.}$ and $y_{c.g.}$ were used to compute E_d according to Eqs. (4.20) - (4.22). Then, correction factors c_L and c_R were computed

according to Eqs. (4.31) and (4.32) and introduced into the odometry program. Similarly the corrected wheelbase b_{new} was computed according to Eqs. (4.24) - (4.26)[2].

[2] Hoping to reduce the effect of non-systematic errors further, we actually computed E_d and E_b in two Hoping to reduce the effect of non-systematic errors further, we actually computed E_d and E_b in two ways:

At this time the calibration procedure was complete. In order to verify the results we ran the UMBmark experiment for a second time, this time with the correction factors in place. Figure 11 shows the results of both the uncalibrated runs and the runs with the calibrated vehicle.

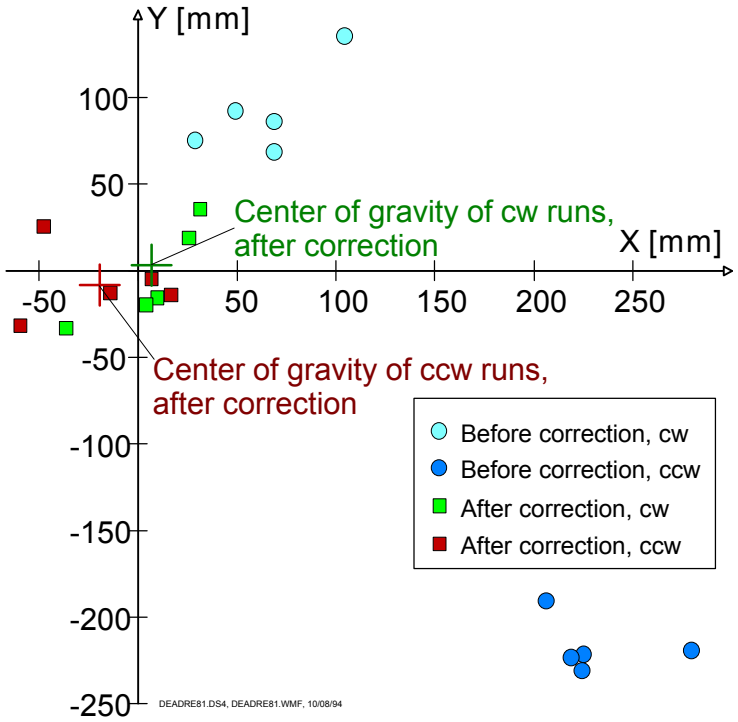

Figure 11: Position Errors after completion of the Bi-directional Square Path Experiment (4 x 4 m).
Before calibration: b=340.00 mm, D_R/D_L = 1.00000
After calibration: b=336.17 mm, D_R/D_L = 1.00084

As explained in Section 3, Eqs. (3.2) and (3.3) were used to express the experimental results quantitatively as the measure of odometric accuracy for systematic errors, $E_{max,syst}$. In the example of Fig. 11, $E_{max,syst}$ was 317 mm before compensation and 21 mm after compensation. This represents a 15-fold improvement.

In order to assure that the experiment shown in Fig. 11 was not an isolated case, we performed another seven carefully monitored experiments. Table I lists the results from all eight experiments. We emphasize that Table I lists all experiments we ever made, it is not a selection of the best runs. We further emphasize that in each experiment we used all runs, without eliminating "outliers" (with the exception of four or five runs where the errors reported by the sonar calibrator were absurdly large, presumably due to a malfunctioning of the sonar calibrator).

The seemingly large fluctuations in improvement, especially among experiments #3, #4, and #5 (which all used the same correction factors) are due to the fact that the centers of gravity (c.g.s) for the runs after calibration are all very close to the origin (as seen in Fig. 11). Thus, the arbitrary spread of return position errors caused by non-systematic error sources has greater impact on the c.g.s. For example, the c.g. of Experiment 4 is only 17 mm (5/8") closer to the origin than the c.g. of Experiment #3 — a difference that is attributed to the arbitrary spread of non-systematic errors.

---

(1) based on the values for $x_{c.g.}$, according to Eqs. (4.20a) and (4.24a); and (2) based on the values for $y_{c.g.}$, according to Eqs. (4.20b) and (4.24b). We then averaged $E_{d,x}$ and $E_{d,y}$, as well as $E_{b,x}$ and $E_{b,y}$. This measure may not be necessary in general, because the respective correction values (based on $x_{c.g.}$ or $y_{c.g.}$) differed by less than 1% in all cases

In principle, it is possible to achieve even better results by performing the compensation procedure for a second time, "on top of" the first compensation. This is so because a compensated robot can be treated as though it was a "new" uncompensated robot, but with different initial parameters. Using the standard deviation (σ) of the 5 runs in each direction it is easy to decide when a second compensation run will be beneficial. The standard deviation of the return position errors in the 4×4 m Bi-directional Square Path Experiment was about 25 mm. The Standard Error of the Mean (SEM), defined as SEM = σ/sqrt(n), was 11.2 mm (n is the number of runs). As a rule-of-thumb sometimes used in small sample statistics [Walpole and Myers, 1985], one can say that if $E_{max,syst} < 3\times SEM$ it is unlikely (here: 5%) that the result can be improved by a second compensation. We put this rule-of-thumb to the test in Experiment #7, where $E_{max,syst}$ = 66 mm was notably worse (the improvement over the uncompensated run was only 6.4-fold) than in the other experiments. Applying the above rule-of thumb, it is evident that 66 mm > 3×SEM = 33.6 mm, so that a second compensation run was indicated. After the second compensation, the vehicle's error was $E_{max,syst}$ = 20 mm, i.e., a 21-fold reduction relative to the uncompensated systematic error.

Table I: The Measure of Odometric Accuracy for Systematic Errors, $E_{max,syst}$, before and after compensation.

Experiment #	$E_{max,syst}$ before compensation [mm]	$E_{max,syst}$ after compensation [mm]	Improvement	Comment
1	317	21	15-fold	Details shown in Fig. 11
2	349	32	11-fold	
3	310	31	10-fold	These 3 experiments used the same set of uncalibrated results and identical correction factors.
4	310	14	22-fold	
5	310	26	12-fold	
6	403	35	11-fold	
7	423	after 1st comp: 66 after 2nd comp: 20	21-fold*	In this experiment the diameter of the right wheel was slightly increased by winding three loops of masking tape around the wheel perimeter.
8	232	12	19-fold	In this experiment the diameter of the left wheel was slightly increased by winding five loops of masking tape around the left wheel perimeter.

*) Two compensation runs were performed. See explanation in main text.

6. CONCLUSIONS

This paper deals with the measurement and correction of systematic odometry errors in differential-drive mobile robots. The paper investigates specifically the errors due to the wheel diameter ratio, E_d, and the uncertainty about the wheelbase, E_b. A third — potentially significant — error is the scaling error, E_s. E_s is the ratio between the average of the actual wheel diameters and the nominal wheel diameter. However, this error is so easy to measure and correct that we have removed it from consideration.

The focus on E_d and E_b is based on our error model, which assumes that systematic orientation errors are either of Type A or Type B. Type A errors are directly affected by E_b and Type B errors are directly affected by E_d. Other systematic errors may also affect the overall Type A and Type B error. However, we do not need to worry about this, because, in principle, both Type A and Type B errors can be eliminated completely by changing the effective wheelbase and wheel-diameter ration in software.

Based on this model we define a benchmark test for odometric accuracy in differential-drive robots. This test, called UMBmark, assures that different odometric errors don't compensate for each other, as may be the case with other odometry tests. The UMBmark procedure yields a single numeric value, $E_{max,sys}$, that represents a quantitative measure of a vehicle's systematic odometry errors. This makes UMBmark an effective tool for evaluating the odometry performance of a vehicle with different parameters and for the comparison of odometry performance between different mobile robots.

Another contribution of this paper is the definition of a systematic procedure for measuring and correcting Type A and Type B odometry errors. The effectiveness of this procedure and the validity of its underlying model are supported by the experimental results. The results show that by changing only the effective wheelbase and the effective wheel-diameter ratio the vehicle's odometric accuracy (with respect to systematic errors only) increased by at least one order of magnitude. This improvement was consistent when tested repeatedly for the same vehicle and when tested on the same vehicle but with artificially altered wheelbases and wheel-diameter ratios.

One should note that odometric calibration factors are used by many researchers. However, to date such factors were usually found by some form of trial-and-error and some intuition on the part of the experimenter. This type of approach is very time consuming and yields inferior results. By contrast, the UMBmark procedure offers a systematic approach that yields near-optimal results. The strength of the UMBmark calibration procedure lies in the fact that even minute mechanical inaccuracies, such as wheel diameters that differ by as little as 0.1% can be isolated and identified. Yet, a conventional measuring tape is all that is needed to conduct the experiment.

With the help of the sonar calibrator the UMBmark procedure lends itself to be implemented as an automated self-calibration procedure. U of M is now beginning to develop such an automated approach. If successful, this method would require only two human interventions: (1) manual measurement of the scaling error E_s (with an ordinary tape measure); and (2) initial placement of the robot in a n L-shaped corner of the testing site. The robot would then run the fully automated

self-calibration routine (UMBmark), compute the calibration factors, and insert the calibration factors into its odometry program. This method should be of interest for all manufacturers of differential-drive autonomous vehicles. Similarly, end-users who are concerned with accurate odometry would want to run the self-calibration routine periodically to correct for different loads and tire-wear.

While the present work reduces only systematic odometry errors, we have recently developed novel odometry methods that can reduce non-systematic odometry errors by two or more orders of magnitude [Borenstein, 1995a, 1995b]. We are currently planning to combine these two methods in a specially designed mobile robot platform. If successful, the combined methods will provide substantially better and more robust odometry for future generations of mobile robots.

Acknowledgments:

This research was funded in part by NSF grant # DDM-9114394 and in part by Department of Energy Grant DE-FG02-86NE37969. The authors wish to thank Mr. Brian Costanza and Mr. Brad Holt for conducting many of the experiments.

---

7. REFERENCES

1. Barshan, B. and Durrant-Whyte, H.F., 1993, "An Inertial Navigation System for a Mobile Robot." Proceedings of the 1st IAV, Southampton, England, April 18-21, pp. 54-59.
2. Barshan, B. and Durrant-White, H. F., 1994, "Orientation Estimate for Mobile Robots Using Gyroscopic Information." 1994 International Conference on Intelligent Robots and Systems (IROS '94). Munich, Germany, September 12-16, pp. 1867-1874.
3. Borenstein, J. and Koren, Y., 1985, "A Mobile Platform For Nursing Robots." IEEE Transactions on Industrial Electronics, Vol. 32, No. 2, pp. 158-165.
4. Borenstein, J. and Koren, Y., 1987, "Motion Control Analysis of a Mobile Robot." Transactions of ASME, Journal of Dynamics, Measurement and Control, Vol. 109, No. 2, pp. 73-79.
5. Borenstein, J., 1993, "Multi-layered Control of a Four-Degree-of-Freedom Mobile Robot With Compliant Linkage." Proceedings of the 1993 IEEE International Conference on Robotics and Automation, Atlanta, Georgia, May 2-7, pp. 3.7-3.12.
6. Borenstein, J., 1994, "The CLAPPER: a Dual-drive Mobile Robot With Internal Correction of Dead-reckoning Errors." Proceedings of the 1994 IEEE International Conference on Robotics and Automation, San Diego, CA, May 8-13, pp. 3085-3090.
7. Borenstein, J., 1995a, "Internal Correction of Dead-reckoning Errors With the Compliant Linkage Vehicle." Journal of Robotic Systems, Vol. 12, No. 4, April 1995, pp. 257-273.

8. Borenstein, J., 1995b, "The CLAPPER: A Dual-drive Mobile Robot With Internal Correction of Dead-reckoning Errors." Video Proceedings of the 1995 IEEE International Conference on Robotics and Automation, Nagoya, Japan, May 21-27, 1995.

9. Borenstein, J., Everett, B., and Feng, L., 1996, "Navigating Mobile Robots: Systems and Techniques." A. K. Peters, Ltd., Wellesley, MA, ISBN 1-56881-058-X, February 1996.

10. Byrne, R.H., KIarer, P.R., and Pletta, J.B., 1992, "Techniques for Autonomous Navigation," Sandia Report SAND92-0457, Sandia National Laboratories, Albuquerque, NM, March.

11. Chenavier, F. and Crowley, J., 1992, "Position Estimation for a Mobile Robot Using Vision and Odometry." Proceedings of IEEE International Conference on Robotics and Automation, Nice, France, May 12-14, pp. 2588-2593.

12. Cox, I. J., 1991, "Blanche — An Experiment in Guidance and Navigation of an Autonomous Robot Vehicle." IEEE Transactions on Robotics and Automation, vol. 7, no. 2, April, pp. 193-204.

13. Crowley, J. L., 1989, "Asynchronous Control of Orientation and Displacement in a Robot Vehicle." Proceedings of the 1989 IEEE International Conference on Robotics and Automation. Scottsdale, Arizona, May 14-19, pp. 1277-1282.

14. Crowley, J. L. and Reignier, P., 1992, "Asynchronous Control of Rotation and Translation for a Robot Vehicle." Robotics and Autonomous Systems, Vol. 10, 1992, pp. 243-251.

15. Cybermotion, 1987, "K2A Mobile Platform." Commercial Sales Literature, 115 Sheraton Drive, Salem, VA 24153.

16. Evans, J. M., 1994, "HelpMate: An Autonomous Mobile Robot Courier for Hospitals." 1994 International Conference on Intelligent Robots and Systems (IROS '94). Munich, Germany, September 12-16, 1994, pp. 1695-1700.

17. Everett, H.R., 1995, "Sensors for Mobile Robots," A K Peters, Ltd., Wellesley, MA, 1995.

18. Feng, L, Koren, Y., and Borenstein, J., 1993, "A Cross-Coupling Motion Controller for Mobile Robots." IEEE Journal of Control Systems. December, pp. 35-43.

19. Gourley, C. and Trivedi, M., 1994, "Sensor Based Obstacle Avoidance and Mapping for Fast mobile Robots." Proceedings of the 1994 IEEE International Robotics and Automation, San Diego, CA, May 8-13, pp. 1306-1311.

20. Hollingum, J., 1991, "Caterpillar make the earth move: automatically." The Industrial Robot, vol. 18, no. 2, pp. 15-18.

21. Komoriya, K. and Oyama, E., 1994, "Position Estimation of a mobile Robot Using Optical Fiber Gyroscope (OFG)." International Conference on Intelligent Robots and Systems (IROS '94). Munich, Germany, September 12-16, pp. 143-149.

22. Kortenkamp, D. et al., 1992, "Integrating Obstacle Avoidance, Global Path Planning, Visual Cue Detection, and Landmark Triangulation in a Mobile Robot." Presented at the 1992 SPIE Symposium on Advances in Intelligent Systems, Mobile Robots VII, Boston, MA, Nov. 15-20.

23. Rencken, W. D., 1994, "Autonomous Sonar Navigation in Indoor, Unknown, and Unstructured Environments."1994 International Conference on Intelligent Robots and Systems (IROS '94). Munich, Germany, September 12-16, pp. 431-438.

24. Skewis T. et al., 1991, "Motion Planning for Hospital Transportation Robot." Proceedings of the 1991 IEEE International Conference on Robotics and Automation, Sacramento, California, April, pp. 58-63.

25. TRC (Transition Research Corporation), Shelter Rock Lane, Danbury, CT, 06810-8159 (Now called HRI – Helpmate Robotics, Inc.).

26. Tsumura T., Fujiwara, N., Shirakawa, T. and Hashimoto, M.: "An Experimental System for Automatic Guidance of Roboted Vehicle Following the Route Stored in Memory." Proc. of the 11th Int. Symp. on Industrial Robots, Tokyo 1981, pp. 18-193.

27. Walpole, R. E. and Myers, R. H., 1985, "Probability and Statistics for Engineers and Scientists," 3rd edition. Macmillan Publishing Company, New York, New York 10022.